D4.3 Operational earthquake loss forecasting for Europe

Deliverable information	
Work package	WP4
Lead	Unina
Authors	E. Chioccarelli A. Pacifico I. Iervolino
Reviewers	[Pasquale Cito and Iunio Iervolino]
Approval	[Management Board]
Status	**Final**
Dissemination level	[internal]
Delivery deadline	30/11/2022
Submission date	[15.12.2022]
Intranet path	[DOCUMENTS/DELIVERABLES/File Name]

This project has received funding from the European Union's Horizon 2020 research and innovation programme under grant agreement No 821115

Table of contents

Summary

MANTIS-K is an operational earthquake loss forecasting (OELF) system developed for Italy. It provides seismic risk metrics (e.g., the expected values of collapsed buildings) at the municipality scale, combining, via a consistent approach, forecasted weekly seismic hazard rates, vulnerability, and inventory models. The seismic hazard rates refer to a grid of point-like seismic sources covering the whole national area and some sea; they are computed by the Italian operational earthquake forecasting system (named OEF-Italy) that provides the expected number of earthquakes exceeding magnitude four, in the week following the analysis. Vulnerability models provide, for defined structural typologies, the conditional probability that an undamaged structure reaches a damage level given the (macroseismic) intensity at the site. Finally, inventory models collect information, at the municipality scale, about the number of buildings in each structural typology. MANTIS-K, in its current version, does not update vulnerability and inventory models after the occurrence of an earthquake and it is not able to account for seismic damage accumulation. These limitations may be relevant during seismic sequences, when earthquakes occur with a short interarrival time. The presented deliverable discusses an improved OELF system, MANTIS v2.0, in which the inventory is updated after each damaging event and possible damage accumulation is considered, profiting from a Markov-chain-based approach to structural reliability. The 2009 L'Aquila sequence is used to compare the losses forecasted by the original and the improved OELF system. The results indicate that damage accumulation can have non negligible effects, as expected, especially in the municipalities within the epicentral area of the earthquakes of the sequences. The differences between the two systems are mitigated for loss forecasting that refers to larger areas, including municipalities far from the earthquakes.

1. Introduction

Operational earthquake forecasting (OEF) is a recently developed branch of seismology that allows to constantly update the short time estimates of seismicity in a region in which the earthquake activity is continuously monitored (Jordan et al., 2011). Although the efficacy of the OEF for seismic risk management and mitigation is currently under debate within the scientific community (e.g., Chioccarelli & Iervolino, 2021; Wang & Rogers, 2014), the possibility of using the information provided by the OEF system for real-time risk assessment and mitigation is worth of investigation.

In Italy, because of the work of the *Istituto Nazionale di Geofisica e Vulcanologia*, a system for operational earthquake forecasting, named OEF-Italy (Marzocchi et al., 2014), exists. It acquires information from the national monitoring network that continuously records the seismic activity in the country. Such information is used to probabilistically forecast the weekly expected number (i.e., rates) and locations of earthquakes with magnitude above a threshold occurring in the monitored area. On the basis of data provided by OEF-Italy, a system for operational earthquake loss forecasting (OELF), named MANTIS-K was developed (Iervolino et al., 2015). MANTIS-K combines the weekly seismicity rates with vulnerability and inventory models for the Italian building stock to obtain weekly forecasts of seismic risk (consequences) metrics, that is, the expected number of collapsed buildings, fatalities, injuries, and displaced residents. However, MANTIS-K has some limitations that may affect the accuracy of the loss forecasting. The system, in its current formulation, adopts vulnerability and inventory models that do not change in time, that is, OEF rates are the only input that change among the loss forecasting computed at different times. This does not appear as an issue in peace conditions (i.e., when no earthquake has recently occurred in the area), but it may affect results right after the occurrence of a damaging earthquake (i.e., during a seismic crisis). Indeed, in such a case, MANTIS-K accounts for the fact that the estimated seismicity in the area increases (e.g., Marzocchi & Lombardi, 2009) but it is not able to model that the structures in the area may have already been damage by previous seismic events. However, seismic crises are the cases in which the social relevance of the OELF results is the highest. Thus, to overcome such limitations, an upgraded version of the system, named MANTIS v2.0, is currently under-development in the context of the ongoing research project RISE (Real-time

earthquake rIsk reduction for a ReSilient Europe). In particular, profiting from the structural reliability model developed for accounting seismic damage accumulation on single structures (Iervolino et al., 2016), this document discusses how the MANTIS-K framework can be modified to account for evolutionary vulnerability models, that is seismic damage accumulation on the existing building portfolio.
The deliverable is structured such that MANTIS-K system is briefly recalled. Then the improved methodology at the base of MANTIS v2.0 is described together with the involved ground-motion and vulnerability models. It follows an application of the updated software to a case study, i.e., a past Italian earthquake sequence that allows to identify some of the differences between the two versions of the software. Final conclusions close the deliverable.

2. MANTIS-K

The OEF-Italy system analyses, continuously in time (t), the data of the recorded seismicity history of the country. Thus, referring to a grid of point-like seismic sources, it provides, for each source $\{x,y\}$, the expected number per unit time (Δt, equal to one week) of earthquakes above magnitude four, originating at the point of interest. These rates, indicated as $\lambda(t,x,y)$, enable to retrieve the expected value of earthquakes per unit time that, in a given area (e.g., a municipality) identified by coordinates $\{w,z\}$, making the building of a structural typology of interest, k, to reach some performance levels of interest, that is, $PL^k = pl_j$. In fact, it is assumed that a finite number, say *n*, of performance levels can be used to discretize the damage conditions of the structure: pl_1 identifies the undamaged state, pl_n the conventional collapse, pl_j, with $j = 2,...,n-1$, the intermediate damages condition between the undamaged and the collapse state (increasing j, the level of damage increases). The sought rate of earthquakes causing a building of the structural typology k, located in $\{w,z\}$, on a soil class indicated as θ, to reach pl_j is $\lambda^k_{PL=pl_j}(t,w,z,\theta)$ and can be computed via Eq. (1):

$$\lambda^k_{PL=pl_j}(t,w,z,\theta) = \int_x \int_y \lambda(t,x,y) \cdot \int_{im=0}^{+\infty} P\left[PL^k = pl_j \middle| im\right] \cdot \int_{m=0}^{+\infty} f_{IM|M,R,\theta}(m,r,\theta) \cdot f_M(m) \cdot dm \cdot dx \cdot dy \,, \quad (1)$$

where M is the magnitude of the earthquake, R is the distance between the point-like seismic source $\{x,y\}$ and the site of interest $\{w,z\}$; $f_M(m)$ is the probability density function of the magnitude of the earthquakes (assumed to be independent and identically distributed among sources); $f_{IM|M,R,\theta}(m,r,\theta)$ is the probability density function (pdf) of the intensity measure, IM, at the site $\{w,z\}$ conditional to $M = m$, $R = r$, and the soil class θ (or possibly other covariates); $P\left[PL^k = pl_j \middle| im\right]$ is the probability that a structure of the *k*-th structural typology reaches pl_j given that $IM = im$ at the construction site (such a probability is assumed independent on θ). $P\left[PL^k = pl_j \middle| im\right]$ can be retrieved by the so-called *fragility functions* for the structural typology of interest. Finally, the integrals over x and y in Eq.(1) are extended to comprehend all the sources within a maximum distance from the $\{w,z\}$ site; such a distance usually depends on the adopted ground motion propagation models providing $f_{IM|M,R,\theta}(m,r,\theta)$.

If the local soil conditions are uncertain, the random variable representing the soil class at the site of the buildings of the structural typology can be considered defining its probability mass function, $P[\theta_q]$, with $q = 1,...,Q$, being Q the number of soil classes. In such a case, the rate of earthquakes taking to pl_j a building randomly selected among those of the structural typology k and located in $\{w,z\}$, i.e., $\lambda^k_{PL=pl_j}(t,w,z)$ can be computed via Eq. (2):

$$\lambda^k_{PL=pl_j}(t,w,z) = \sum_{q=1}^{Q} P[\theta_q] \cdot \lambda^k_{PL=pl_j}(t,w,z,\theta_q) \,. \quad (2)$$

In the same hypotheses discussed in Iervolino et al. (2015), if the number of building of the *k*-th structural typology at $\{w,z\}$ site is available, $N^k_B(w,z)$, the expected number of buildings reaching pl_j in $(t,t+\Delta t)$, that is $N^k_{B,pl_j}(t+\Delta t,w,z)$, can be approximately computed via Eq. (3):

$$N^k_{B,pl_j}\left(t+\Delta t,w,z\right)\approx N^k_B\left(w,z\right)\cdot\lambda^k_{PL=pl_j}\left(t,w,z\right)\cdot\Delta t\ . \tag{3}$$

3. MANTIS v2.0

The upgraded version of the OELF system is formulated to account for the evolution, over time, of the structural damage conditions. This implies that loss forecasting must account for the possible structural damage accumulation due to the occurrence of more than one earthquake in the forecasting period. Moreover, the upgraded system has to estimate the possible damage due to the occurred earthquakes and, consequently, forecast the performance level of buildings that, at the time of computation, are already at an intermediate performance level. In the following, the loss forecasting referring to a building inventory constituted by already damaged buildings is discussed first. Then, the possible structural damage accumulation due to the occurrence of more than one earthquake in the forecasting time window is analysed. Finally, the adopted strategy for updating the inventory to account for the damage evolution in the sequence is described.

3.1 Loss forecasting referring to already damaged buildings

In order to account for damage accumulation, some hypotheses about the structural damage evolution over time have to be introduced. More specifically, it is assumed that, for each building of the considered structural typology, the probability to pass from pl_i with $i=1,\ldots,n-1$ to another (worse) performance level, pl_j with $i<j\le n$, due to one earthquake does not depend on the damage history of the structure, but it only depends on pl_i and on the intensity of the earthquake possibly causing the transition, that is im. This enables adopting a Markov-chain model, in analogy with Iervolino et al. (2016), to compute the probability that a structure, located at the $\{w,z\}$ site, passes from pl_i to pl_j $(j>i)$ given the occurrence of a *generic* earthquake (an earthquake of unspecified magnitude and location), indicated as $P^k_{i,j}\left(t,w,z\right)$, is computed as per Eq. (4):

$$\begin{aligned}&P^k_{i,j}\left(t,w,z\right)=\\&=\sum_{q=1}^{Q}P\left[\theta_q\right]\cdot\int_{im=0}^{+\infty}P\left[PL^k=pl_j\middle|pl_i,im\right]\cdot\iint_{x\ y}\frac{\lambda\left(t,x,y\right)}{\nu\left(t,w,z\right)}\cdot\int_{m=0}^{+\infty}f_{IM|M,R,\theta}\left(im\middle|m,r,\theta_q\right)\cdot f_M\left(m\right)\cdot dm\cdot dx\cdot dy\cdot d\left(im\right)\end{aligned}\ . \tag{4}$$

In the equation, $P\left[PL^k=pl_j\middle|pl_i,im\right]$ is the probability the structure makes a transition from pl_i to pl_j for a given value of IM. Such a probability can be evaluated, via Eq. , as the difference between two probabilities, both conditional on the value of the intensity measure and the performance level pl_i in which the structure is before the earthquake occurrence; such conditional probabilities are those of reaching or exceeding pl_j and pl_{j+1}, respectively and are defined as state-dependent fragility functions (Iervolino et al., 2016). Finally, $\lambda\left(t,x,y\right)/\nu\left(t,w,z\right)$ is the probability that, given that an earthquake affects the $\{w,z\}$ site, it is generated by the $\{x,y\}$ source; $\nu\left(t,w,z\right)$ is the rate of the earthquakes affecting the $\{w,z\}$ site and can be computed as shown in Eq. (5):

$$\nu\left(t,w,z\right)=\iint_{x\ y}\lambda\left(t,x,y\right)\cdot dx\cdot dy\ . \tag{5}$$

A matrix collecting all the transition probabilities of the same structural typology at $\{w,z\}$ site given the occurrence of an earthquake, $\left[P^k\left(t,w,z\right)\right]$, can be defined as in Eq. (6) (for the sake of simplicity, the dependency on $\{w,z\}$ and time is neglected for the terms within the matrix):

$$\left[P^k\left(t,w,z\right)\right]=\begin{bmatrix}1-\sum_{j=2}^{n}P^k_{1,j} & P^k_{1,2} & \cdots & \cdots & P^k_{1,n}\\ 0 & 1-\sum_{j=3}^{n}P^k_{2,j} & \cdots & \cdots & P^k_{2,n}\\ \cdots & \cdots & \cdots & \cdots & \cdots\\ 0 & \cdots & 0 & 1-P^k_{(n-1),n} & P^k_{(n-1),n}\\ 0 & \cdots & \cdots & 0 & 1\end{bmatrix}\ . \tag{6}$$

The matrix has $n \times n$ dimension and the element at row i and column j is the probability that, due to a generic earthquake, one structure of the *k*-th typology, that is in pl_i before the earthquake, goes to pl_j due to the earthquake occurrence. Thus, $\left[P^k(t,w,z)\right]$ is an upper triangular matrix because the structure cannot lower its performance level due to an earthquake occurrence.

The unit time transition probability matrix for the structural typology, $\left[P_E^k(t,t+\Delta t,w,z)\right]$, collecting the transition probabilities from one damage state to another in Δt, can be computed. Assuming that, in the unit time, the process of earthquake occurrence can be approximated by a homogeneous Poisson Process, HPP, (in analogy with what was discussed for MANTIS-K), if $\nu(t,w,z)$ is small (i.e., the probability of more than one earthquake in Δt is negligible), the matrix $\left[P_E^k(t,t+\Delta t,w,z)\right]$ can be approximated via Eq. (7):

$$\left[P_E^k(t,t+\Delta t,w,z)\right] \approx \nu(t,w,z)\cdot\left[P^k(t,w,z)\right] + \left\{1-\nu(t,w,z)\right\}\cdot[I], \quad (7)$$

where $\nu(t,w,z)$ approximates the probability of one earthquake occurrence in the unit time, $\left\{1-\nu(t,w,z)\right\}$ approximates the probability of no earthquake in the unit time and $[I]$, the identity matrix, accounts for the fact that, when no earthquake occurs, the building does not change its performance level.

Once $\left[P_E^k(t,t+\Delta t,w,z)\right]$ is known, the expected number of buildings in each damage state at time $(t+\Delta t)$ can be computed knowing the number of buildings in each damage state at time t (see Section 3.3). More specifically, let us assume that $\mathbf{N}_B^k(t,w,z)$ is the vector collecting the number of the buildings of the *k*-th structural typology located in $\{w,z\}$ at the time *t*, the expected number of buildings in each performance level at $(t+\Delta t)$, $\mathbf{N}_B^k(t+\Delta t,w,z)$, is provided by as:

$$\mathbf{N}_B^k(t,w,z)\cdot\left[P_E^k(t,t+\Delta t,w,z)\right] = \left\{N_{B,pl_1}^k(t,w,z), N_{B,pl_2}^k(t,w,z),..., N_{B,pl_n}^k(t,w,z)\right\}\cdot\left[P_E^k(t,t+\Delta t,w,z)\right]. \quad (8)$$

Indeed, in Eq. (8), the transition probabilities from a starting damage state to an arriving one are multiplied by the corresponding number of buildings in the starting damage state. Eq. (8) in MANTIS v2.0 substitutes the corresponding Eq. (3) implemented in MANTIS-K.

3.2 Loss forecasting accounting for more than one earthquake

Depending on the seismic history, the rates of OEF may result in a value of $\nu(t,w,z)$ that corresponds to a non-negligible probability of more than one earthquake in Δt. In this case, the approximation introduced in Eq. (7) is not acceptable, but the application of the described Markovian approach remains possible if the original unit time, i.e. one week, is partitioned into smaller intervals such that, in each of them, the probability of more than one earthquake is negligible. Thus, the way in which the original Δt has to be partitioned depends on the distribution of the number of expected earthquakes over time. Once the length of the new time intervals is defined, Eq. (7) can be applied for each of them and the transition probability matrix referred to one week can be computed proofing of the Markov-chain properties. The resulting transition probability matrix will account for the possible damage accumulation due to multiple forecasted earthquakes in one week.

3.3 Inventory update

After the occurrence of each earthquake, it is important to update the $\mathbf{N}_B^k(t,w,z)$ vector to apply Eq. (8). To this aim, let us assume that the observed IM at the $\{w,z\}$ site, im^*, is known; the probability that the building in the *k*-th structural typology passed from pl_i to pl_j due to im^*, $P_{i,j}^{k*}(w,z)$, can be derived by the already introduced state-dependent fragility functions, as $P\left[PL^k = pl_j \middle| pl_i, im^*\right]$.

In fact, the value of im^* is known if an accelerometric station provides the recorded ground motion at $\{w,z\}$ site. If such a data is not available, it is possible to compute a distribution of the intensity measure of interest at $\{w,z\}$ conditional to the earthquake magnitude, m^*, the distance

between the earthquake and the site, r^*, the soil class, θ_q, (and possibly information from ground motion recorded at other sites), that is $f_{IM|M,R,\theta}\left(im\middle|m^*,r^*,\theta_q\right)$ (e.g., Wald et al. 1999; Worden et al. 2020). Thus, it is sufficiently general to assume that, although the im^* value is unknown in $\{w,z\}$, $P_{i,j}^{k*}(w,z)$ can be obtained via Eq. (9):

$$P_{i,j}^{k*}(w,z)=\sum_{q=1}^{Q}P\left[\theta_q\right]\cdot\left\{\int_{im=0}^{+\infty}P\left[PL^k=pl_j\middle|pl_i,im\right]\cdot f_{IM|M,R,\theta}\left(im\middle|m^*,r^*,\theta_q\right)\cdot d(im)\right\}. \quad (9)$$

A transition probability matrix given the occurrence of the earthquake of m^* magnitude and r^* distance can be defined by collecting the values of $P_{i,j}^{k*}(w,z)$ for both i and j varying between 1 and n, as per Eq. (10):

$$\left[P^{k*}(w,z)\right]=\begin{bmatrix}1-\sum_{j=2}^{n}P_{1,j}^{k*} & P_{1,2}^{k*} & \cdots & \cdots & P_{1,n}^{k*}\\ 0 & 1-\sum_{j=3}^{n}P_{2,j}^{k*} & \cdots & \cdots & P_{2,n}^{k*}\\ \cdots & \cdots & \cdots & \cdots & \cdots\\ 0 & \cdots & 0 & 1-P_{(n-1),n}^{k*} & P_{(n-1),n}^{k*}\\ 0 & \cdots & \cdots & 0 & 1\end{bmatrix}. \quad (10)$$

Moreover, if more than one earthquake occurs in the Δt, say $n_E=\{1,\ldots,N_E\}$, a transition probability matrix per event can be defined, $\left[P_{n_E}^{k*}(w,z)\right]$, in accordance with Eq. (10). The cumulative effect of the N_E earthquakes can be computed by multiplying the corresponding transition probability matrices. Thus, the vector collecting the estimated number of buildings in each damage state, $\mathbf{N}_B^k(t,w,z)$, can be obtained from the equivalent vector estimated in the previous time interval at the same site, $\mathbf{N}_B^k(t-\Delta t,w,z)$, via Eq. (11):

$$\mathbf{N}_B^k(t,w,z)=\mathbf{N}_B^k(t-\Delta t,w,z)\cdot\prod_{n_E=1}^{N_E}\left[P_{n_E}^{k*}(w,z)\right]. \quad (11)$$

The computed $\mathbf{N}_B^k(t,w,z)$ is the one adopted in Eq. (8), i.e., an input value for the operational earthquake loss forecasting as discussed in Section 3.1.

4. CASE STUDY

In this deliverable, L'Aquila 2009 seismic swarm is retrospectively analysed by means of MANTIS v2.0. The characteristics of the seismic sequence are described hereafter together with the models adopted for MANTIS- v2.0 implementation. The discussion of results is reported in Section 5.

The mainshock (moment magnitude, M, 6.1) of the swarm struck the region at 01:32 a.m. of the 06/04/2009 and, from January 2009 to June 2010, a sequence of twenty-four earthquakes with moment magnitude larger than 4.0 occurred, within 50 km from the mainshock epicentre (Chiocarelli & Iervolino, 2010). Among them, those with moment magnitude larger than 4.5 were eight (excluding the mainshock), all of them occurred after the mainshock is a short time interval ranging between the 06/04/2009 and 10/04/2009. Table 1 reports the coordinates of the epicentres and the magnitudes of the mainshock and of the eight M4.5 subsequent earthquakes.

Table 1. Earthquakes with moment magnitude larger than 4.5 identified by a progressive number (ID), latitude and longitude, in degree, and M.

Date [dd/mm HH:MM]	ID	Latitude [°]	Longitude [°]	M
06/04 01:32	1	42.342	13.380	6.1
06/04 02:37	2	42.360	13.328	5.1
06/04 03:56	3	42.335	13.386	4.5
06/04 23:15	4	42.463	13.385	5.1
07/04 09:26	5	42.336	13.387	5.1

07/04 17:47	6	42.303	13.486	5.5
07/04 21:34	7	42.372	13.374	4.5
09/04 00:53	8	42.489	13.351	5.4
09/04 19:38	9	42.504	13.350	5.2

The results of the OELF procedure are discussed considering a time window of five days ranging from the 05/04/2009 (i.e., one day before the mainshock) to 10/04/2009. It is (arbitrarily) assumed that earthquakes with magnitude lower than 4.5 produced negligible damages of the existing buildings. Thus, the updating of the building portfolio is performed considering the same earthquakes listed in Table 1. The OELF results are computed for all the municipalities that are within 100km from the epicentre of the mainshock grouped in four sets characterized by increased distance from the mainshock. More specifically, as shown in Figure 1, the first set is constituted by the two municipalities within 10 km from the mainshock, the second set consists of 66 municipalities within 40 km; the third and the fourth sets are constituted by 283 and 598 municipalities that are within 70 km, and 100 km from the mainshock, respectively. In Figure 1 the epicentres of the considered earthquakes are also reported with the same ID defined in Table 1.

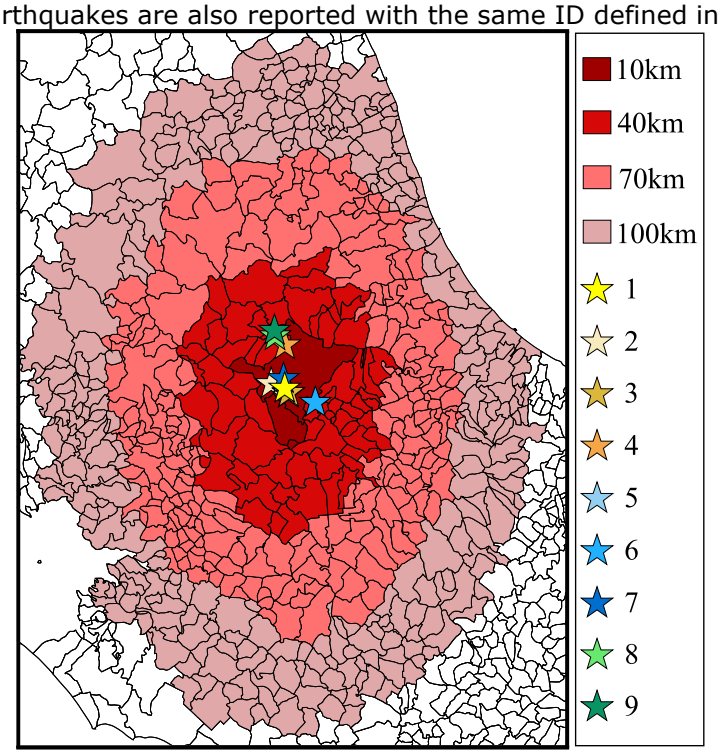

Figure 1. Map of considered municipalities grouped for the increasing distance from the mainshock; the stars represent the epicenters of the earthquakes of Table 1.

4.1 Input models

Models implemented in the development of MANTIS v2.0 are described in the following. In Section 4.1.1 the adopted hazard models are reported; fragility and exposure models are discussed in Section 4.1.2 and Section 4.1.3, respectively; Section 4.1.4 deals with the local soil model to evaluate the soil probabilities. Finally, in Section 4.1.5 the damage assessment model, involved in the inventory updated is explained.
Moreover, these models will be involved in Eq. (1) too (replacing those described in Iervolino et al., 2015), in an update version of MANTIS-K, named MANTIS-K v1.1, that will be used for comparing the obtained results.

4.1.1 Hazard models

The short-term hazard modelling relies on the OEF-Italy forecasted rates $\lambda(t,x,y)$. The numerical values of the OEF rates released by OEF-Italy at midnight of the six days of interest are represented in Figure 2. As already discussed in literature (Marzocchi et al., 2014), rates from OEF

significantly increase right after strong earthquakes: in the considered cases, the maximum value of $\lambda(t,x,y)$ in the region of the sequence at 05/04 and 06/04 is about 5E-3, whereas, at 07/04 (i.e., the first forecasting after the mainshock) it increases up to 5E-2.
For each point-like seismic source, the pdf of the generated magnitude, $f_M(m)$, is derived from the Gutenberg–Richter relationship (Gutenberg & Richter, 1944) with unbounded maximum magnitude and b-value equal to one. At the site of interest $\{w,z\}$, the conditional distribution of the intensity measure $f_{IM|M,R,\theta_q}(im|m,r,\theta_q)$ is computed proofing of the ground motion prediction equation (GMPE) of Bindi et al. (2011).
To be consistent with the fragility models (described in the next section), the geometric mean of the pseudo-spectral accelerations, $Sa(T)$, over a range of spectral periods is chosen as intensity measure (Baker & Cornell, 2006). Such an intensity measure, denoted as $Sa_{avg}(\mathbf{T})$, is defined by Eq. (12):

$$Sa_{avg}(\mathbf{T}) = \sqrt[L]{\prod_{l=1}^{L} Sa(T_l)}\,, \tag{12}$$

The vector $\mathbf{T}$ collects the twenty-three vibration periods considered in Bindi et al. (2011) GMPE: T={0, 0.04, 0.07, 0.1, 0.15, 0.2, 0.25, 0.3, 0.35, 0.4, 0.45, 0.5, 0.6, 0.7, 0.8, 0.9, 1, 1.25, 1.5, 1.75, 2, 2.5, 2.75}s, where $Sa(0s)$ represents the peak ground acceleration or PGA. Since the chosen GMPE does not directly provide the conditional distribution of $Sa_{avg}(\mathbf{T})$, the way in which such a distribution can be computed is discussed in Appendix A.

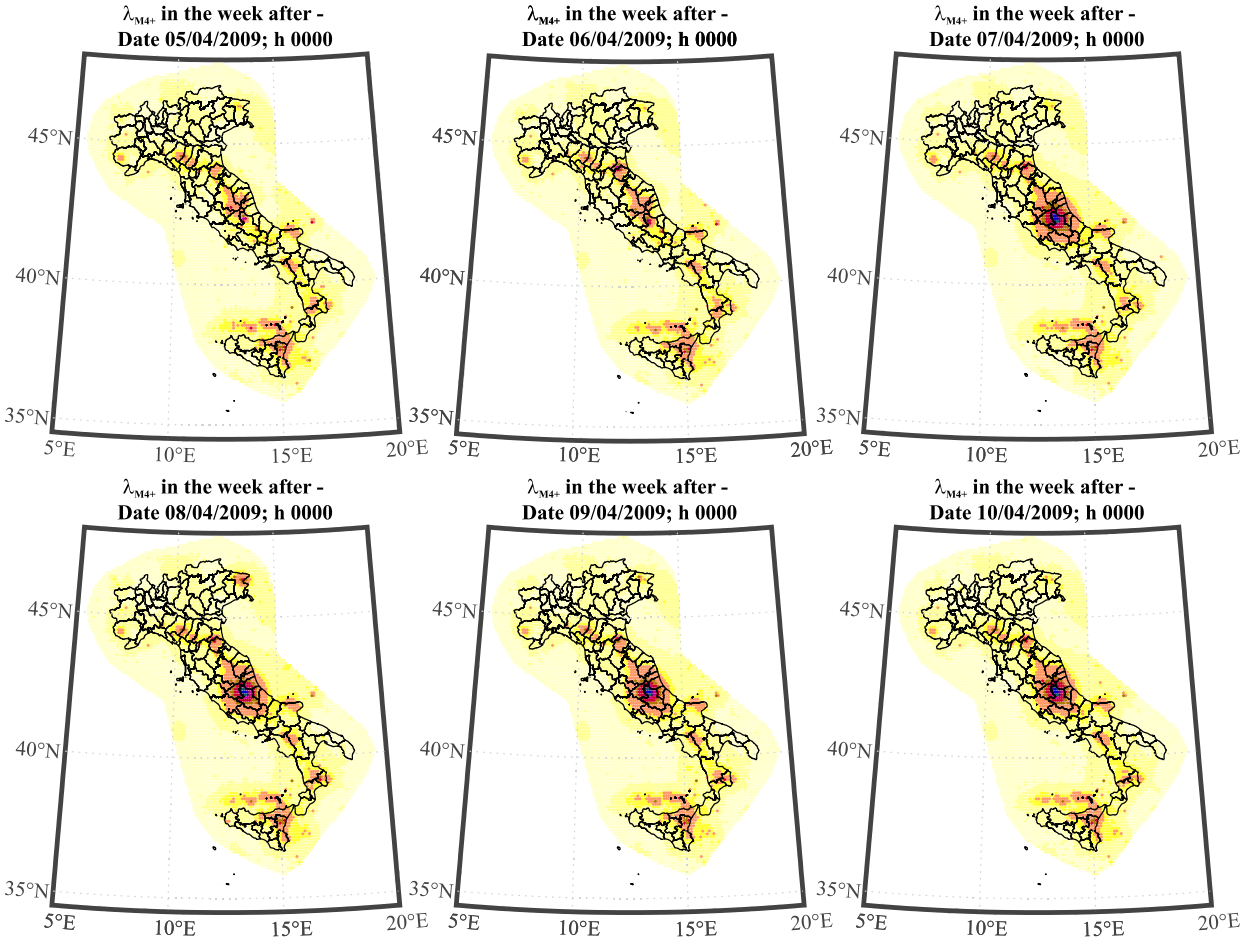

Figure 2. OEF-Italy weekly rate release from 05/04/09 to 10/04/09.

4.1.2 Fragility models

In a recent European research project, SERA (Seismology and Earthquake Engineering Research Infrastructure Alliance for Europe), a building taxonomy and the corresponding structural models

representative of the European existing structures was developed (Romão et al., 2019). They consider four main characteristics: (i) primary construction material (e.g., reinforced concrete (CR), unreinforced masonry made up by clay brick masonry (CL99), dressed stone masonry (STDRE), rubble stone masonry (STRUB), confined masonry (MCF), steel, etc.), (ii) typology of the lateral load resisting system (e.g., wall, moment frame, infilled frame, etc.), (iii) height expressed in terms of number of stories, (iv) seismic capacity-related properties (e.g., ductility and/or design later force), which depend on the evolution of seismic design in the country. Hereafter, the models associated to the Italian residential buildings are considered; that is, ten unreinforced masonry structures characterized by three stone typologies, five reinforced masonry structures, and eighteen reinforced concrete infilled frame structures with design lateral force coefficient, a, equal to 0 or 5. Masonry building typologies are characterized by a number of stories between one and five, whereas the height of reinforced concrete structures varies between one a six stories. Further details about the structural configuration are provided in Appendix B.
Each structural typology is modelled via equivalent single-degree-of-freedom systems or ESDoF (e.g., Suzuki & Iervolino, 2019) characterized by piece-wise linear backbone curves and a pinched hysteretic behavior exhibiting degradation of strength and of (unloading and reloading) stiffness under cyclic loading. Moreover, four damage thresholds were also defined in the SERA project on the basis of Villar-Vega et al. (2017) and Lagomarsino & Giovinazzi (2006) identifying five performance levels: undamaged, slight damage, moderate damage, extensive damage and collapse. Finally, Orlacchio et al. (2021) developed fragility functions and state-dependent fragility functions for each structural typology and performance level; the adopted intensity measure is $Sa_{avg}(\mathbf{T})$ as defined in Eq. (12). Resulting state-dependent fragility functions are lognormal distributions, $\Phi[\bullet]$, with η and β parameters, as per Eq.(13):

$$P\left[PL^k \geq pl_j \middle| pl_i, IM = im\right] = \Phi\left[\left(\ln(im) - \eta\right)/\beta\right]. \quad (13)$$

The values of η and β parameters for all the structural typologies are reported in Appendix B.

4.1.3 Exposure models

SERA project provides, for several European countries, the composition of the residential building stock at municipality scale. Thus, for each Italian municipalities, the number of the buildings of the *k*-th structural typology, N_B^k of Eq. (8), is available.

Figure 3 depicts the composition of the building stock of the considered sets of municipalities. As it regards the CR structures, they have been divided according to the value of the design lateral force coefficient, thus $\alpha \neq 0$ and $\alpha = 0$ denote the absence or the presence of the seismic design, respectively. Residential buildings of the two municipalities within 10 km from the mainshock, are 15373; 63% of them are STRUB structures, 27% are CR structures with seismic design, 8% are MCF structures and there are no CR structures without seismic design. If the municipalities within 40 km, 70 km and 100 km are considered, the total number of residential buildings is 85458, 274445 and 685898 respectively. The percentage of the STRUB structures remains quite constant for all the considered municipalities, equal to about 75%; on the other hand, the percentage of RC structures with seismic design for municipalities within 40 km, 70 km and 100 km is 18%, 15%, 11% respectively. Referring to the set of 598 municipalities, 9% of the residential buildings is constituted by RC structures without seismic design, while this structural typology represents only 3% of the building portfolio when municipalities within 70 km are considered. Finally, the percentage of RC structures without seismic design becomes negligible when municipalities within 40 km are considered. In other words, the figure shows that, as expected, a large majority of Italian residential buildings are masonry buildings and RC structures are mostly located in the largest towns that, in the considered area, are represented by L'Aquila.

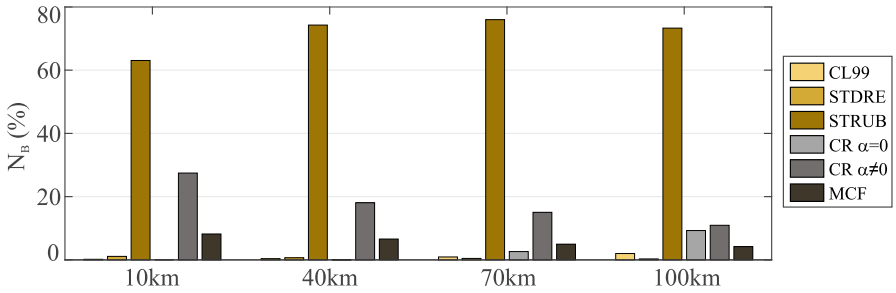

Figure 3 Composition of the building stock according to the construction material.

4.1.4 Local soil models

To apply Eqs. (2) and (4), the $P\left[\theta_q\right]$ probability has to be computed, at the municipality scale, for each soil class. More specifically, such a probability is computed referring to the urbanized areas of each municipality. They are derived by the data of the *Italian Istituto Nazionale di Statistica* (ISTAT) that classifies the Italian municipalities in four classes: city centres, built areas, industrialized areas and sparse buildings areas. The first two are considered as urbanized area (an analogous procedure was adopted in Pacifico et al., 2022). To compute $P\left[\theta_q\right]$, the grid of soil classes provided by Forte et al. (2019) is superimposed, in area of interest, to the map of urbanized areas. Thus, for each municipality, defining the total number of points within the urbanized areas, N_{urb}, and the number of points of a specific soil classes, N_{θ_q}, $P\left[\theta_q\right]$ is computed as per Eq. (14), where $\theta_1, \theta_2, \theta_3, \theta_4$ correspond in turn to soil classes A, B, C, D of Bindi et al. (2011) GMPE:

$$P\left[\theta_q\right] = \frac{N_{\theta_q}}{N_{urb}}, \qquad q = \{1,\ldots,4\}. \tag{14}$$

In Figure 4 the values of $P\left[\theta_q\right]$ are reported per municipality. In accordance with the findings of Pacifico et al. (2022), soil class B is the most representative of the urbanized areas. A medium-to-low percentage of soils C and A is computed, whereas soil class D is generally low.

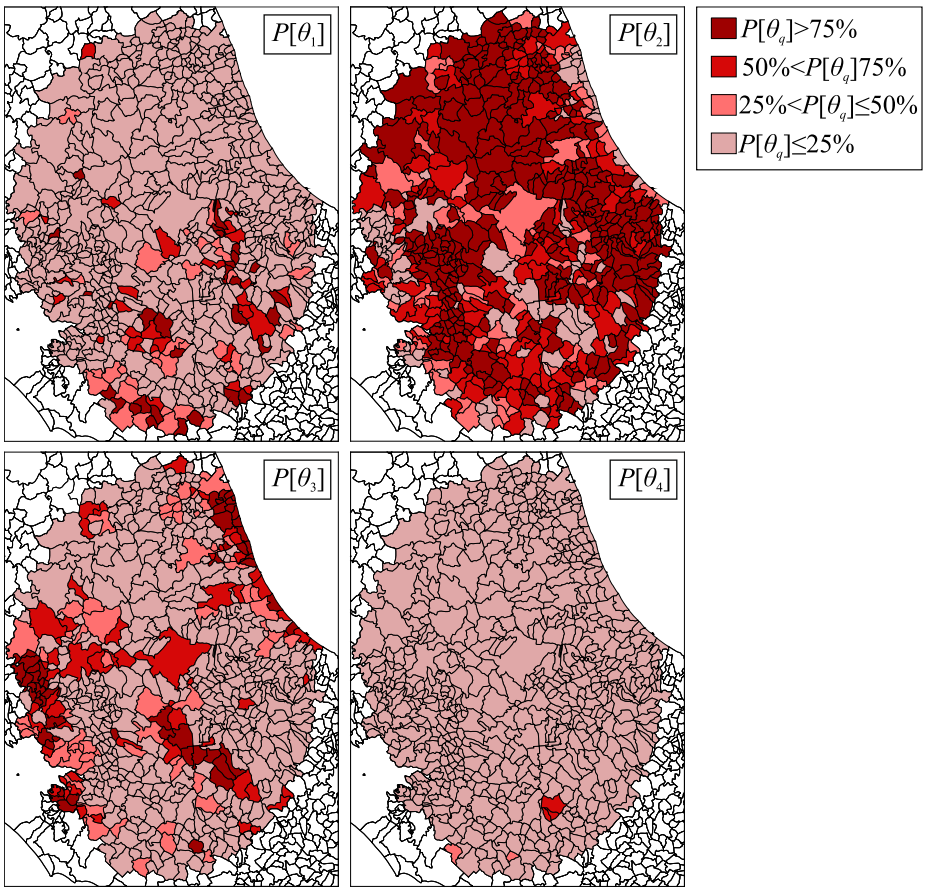

Figure 4 Soil probabilities in the municipalities within 100km from L'Aquila 2009 mainshock.

4.1.5 Damage assessment models

To update the building portfolio as per Eq. (11), the ground motion intensity of the occurred earthquakes is required for all the sites of interest $\{w,z\}$. The required IM is the $Sa_{avg}(\mathbf{T})$ defined as per Eq. (12). Although the latter is usually not directly available (it can be directly computed only if an accelerometric station recorded the effect of the earthquake in the site of interest), this information can be retrieved from ShakeMaps (Worden et al., 2020) that, starting from the data recorded by the Italian seismic network and the source type model of (Wald et al., 1999)[1], provides the expected values (and sigma) of some IMs (PGA, $Sa(0.3s)$, $Sa(1s)$, $Sa(3s)$ and peak ground velocity, PGV) for a grid of points covering a large area around the earthquake source. As an example, the ShakeMap in terms of PGA, $Sa(0.3s)$ and $Sa(1s)$, released after the mainshock of the L'Aquila sequence and available at http://shakemap.ingv.it/shake4.
Indeed, it is possible to demonstrate that, in each point of the grid, ShakeMap data can be used to retrieve the mean, and standard deviation of the logarithms of the Sa_{avg} evaluated over the periods $\mathbf{T}$, conditioned to the occurrence of the Sa_{avg} evaluated over the periods $\mathbf{T}^*=\{0,0.3,1\}$ s (i.e., the data of the ShakeMap), $\ln Sa_{avg}(\mathbf{T}^*)=\chi$. The mean, $E\left[\ln Sa_{avg}(\mathbf{T})\,|\,m^*,r^*,\theta,\chi\right]$, depends on the magnitude of the occurred earthquake m^*, the Joyner-Boore distance r^*, the local soil condition θ and χ; the standard deviation, $\sqrt{VAR\left[\ln Sa_{avg}(\mathbf{T})\,|\,\chi\right]}$, only takes into account for the Sa_{avg} evaluated over the periods of the vector $\mathbf{T}^*$ (see Appendix A for further details).
Assuming a lognormal distribution, for each grid point of the ShakeMap, the conditional probability $f_{IM|M,R,\theta,X}\left(im\middle|m^*,r^*,\theta_q,\chi\right)$, can be computed. However, in accordance with Eq. (9), a transition probability for the each municipality, $P_{i,j}^{k^*}(w,z)$, is required. To obtain such a value, assuming that

[1] It has to be highlighted that the soil characterization provided by the ShakeMap are consistent with Forte et al. (2019). Indeed, the latter is an upgrade of the work of *Istituto Superiore per la Protezione e la Ricerca Ambientale* (Wald et al., 1999), ShakeMap are basing on.

multiple ShakeMaps values say, $n_p = \{1,...,N_P\}$, are available for the municipality, Eq. (9) can be applied in each of the N_P points of the ShakeMaps providing different values of $P_{i,j}^{k*}(w,z)_{n_p}$ due to different soil conditions (in principle, each point is also characterized by a different value of r^* but such an effect is considered to be minor). Thus, the value of $P_{i,j}^{k*}(w,z)$ the whole municipality, can be computed as:

$$P_{i,j}^{k*}(w,z) = \sum_{n_P=1}^{N_P} P_{i,j}^{k*}(w,z)_{n_p} \cdot \frac{1}{N_P}. \quad (15)$$

Finally, $P_{i,j}^{k*}(w,z)$ can be used for the construction of $\left[P^{k*}(w,z)\right]$ of Eq. (10).

5. Results

Both MANTIS-K v.1.1 and MANTIS v2.0 systems are (retrospectively) applied to L'Aquila 2009 seismic swarm. Forecasted losses computed at midnight of each day from 05/04/2019 to 10/04/2009 are presented and discussed referring to the percentages of damaged buildings. Although both the systems provide results at the municipality scale, in the following sections, the quantitative comparison between MANTIS-K v.1.1 and MANTIS v2.0 refers to results for larger areas, that is, all the municipalities within 10, 40, 70 and 100 km from the mainshock epicentre.

5.1 MANTIS-K v1.1

Figure 5 shows results of MANTIS-K v.1.1. In the figure, the panels from a) to d) shows the aggregated results for municipalities within 10, 40, 70 and 100 km from the epicentre of the mainshock; the results are in terms of the forecasted number of buildings in each PL as a function of the day of analysis. Due to the discussed limitation of the first formulation of the OELF system, the differences between the results of different days are only due to the characteristics of the OEF rates. Thus, regardless the extension of the considered area, the expected losses are negligible in the days before the mainshock (99.9% of undamaged buildings), i.e., the 5th and the 6th of April. Indeed, as also shown in Figure 2, before the occurrence of the mainshock, the OEF rates in the considered area were in accordance with those provided in other Italian areas characterized by large seismicity in long term conditions. This is a known characteristic of the OEF models (e.g., Iervolino et al., 2015; Marzocchi et al., 2015).
Results associated to the 7th of April, i.e., when the OEF-Italy rates increase due to the occurrence of the M6.1 earthquake, strongly depend on the considered area. If the two municipalities within 10km are taken into account, the 94% of the structures are forecasted to be undamaged, the 2% are expected to be in pl_5, the 3%, 1%, and 0% belong to the intermediate performance levels, i.e., pl_2, pl_3 and pl_4 respectively. By enlarging the area up to 40 km, 70 km or 100 km, the percentage of the expected undamaged buildings passes to 97%, 99%, and 99% respectively; the 1%, 1%, and 0% of the buildings are expected to be in pl_2; the 0%, of the buildings are expected to be in pl_3 and pl_4 (regardless the distance from the epicenter of the mainshock); the 1% of the building are expected to be in pl_5 whereas 0% are expected in the same performance level when municipalities within 70 km and 100 km from the mainshock are considered. The results computed in the subsequent days are with those computed on the 7th due to the characteristics of the OEF rates.

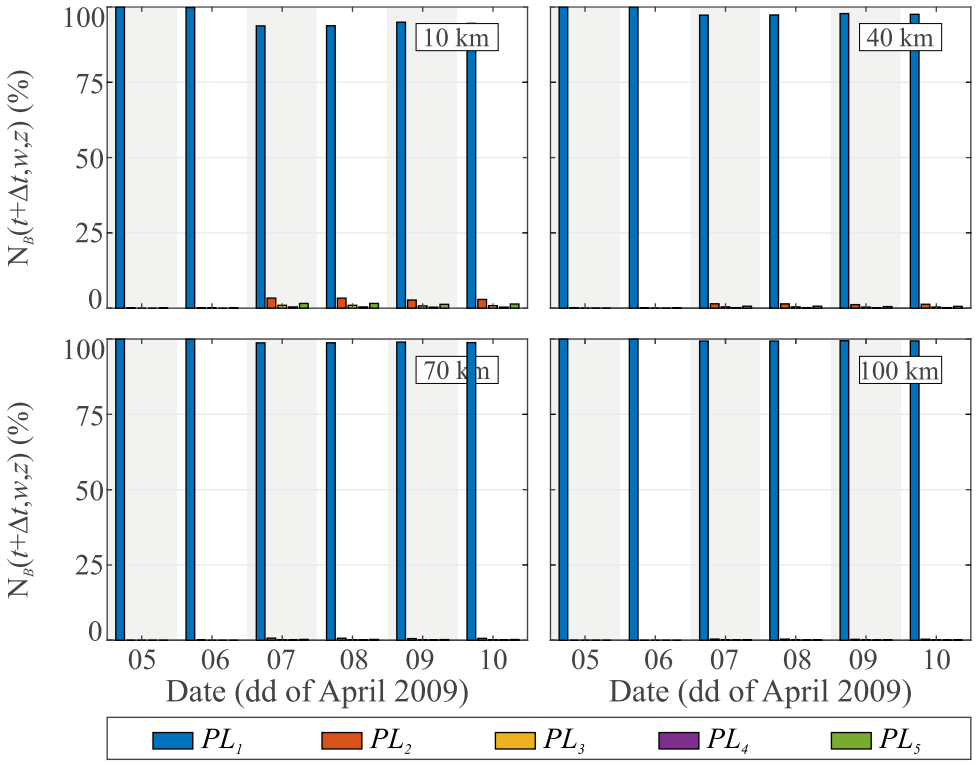

Figure 5. Outcomes of MANTIS-K v.1.1 system applied to 2009 L'Aquila seismic sequence.

5.2 MANTIS v2.0

In this section the results of MANTIS v2.0 are reported considering the same seismic sequence. In accordance with Figure 5, Figure 6 shows the expected number (in percentage) of buildings in each damage condition for the municipalities within 10, 40, 70 and 100 km from the epicentre of the mainshock. Similarly, to the already discussed results of MANTIS-K v.1.1, when results refer to the rates of the 5th and the 6th of April, a few buildings are expected to collapse (less than 1% in the municipalities closest to the mainshock epicentre, i.e., about 8 building over 15373 when the municipalities within 10km are considered). The results of the 7th of April depend on the considered area: the percentages of the expected undamaged buildings are 6% (i.e., about 900 buildings), 44%, 78% and 91% for the municipalities within 10 km, 40 km, 70 km and 100 km from the mainshock, respectively. Still referring to the 7th of April, the expected percentages of buildings in the intermediate *PL*s provided by MANTIS v2.0 are lower than the counterpart evaluated via MANTIS-K v.1.1 and the percentage of the buildings expected to be in pl_5 by MANTIS v2.0 are always larger than those evaluated by neglecting damage cumulation (67%, i.e., about 10334 buildings, 21%, 7% and 3% for 10 km, 40 km, 70 km and 100 km, respectively), as expected. More specifically, the differences between the forecasted percentages of conventionally collapsed buildings according to MANTIS-K v.1.1 and MANTIS v2.0 are 65%, 20%, 7%, and 3% for municipalities within 10, 40, 70 and 100km. Thus, differences between results of the two systems are more significant in the epicentral areas and tend to be negligible increasing the extension of the area of interest.

Results of MANTIS v2.0 for the days from the 8th to the 10th of April, are in good accordance with those of the 7th of April.

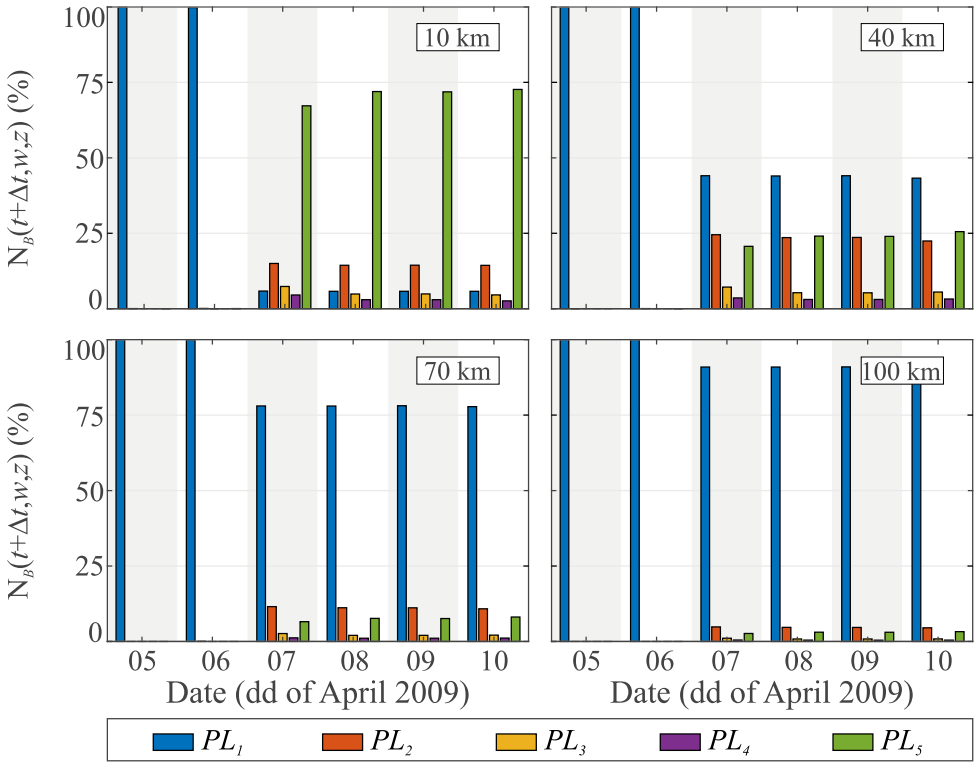

Figure 6. Outcomes of MANTIS v2.0 system applied to 2009 L'Aquila seismic sequence.

To deepen the comparison between the two version of MANTIS, Figure 7 shows the percentage number of buildings in each *PL* computed by MANTIS v2.0 in accordance with the available information about the already occurred earthquakes, i.e., by applying Eq. (11). Thus, it should be underlined that, although the format of Figure 7 is the same of Figure 5 and Figure 6, the values reported in Figure 7 are not the results of an operational forecasting; they represent the estimated damage conditions of the building portfolio that MANTIS v2.0 adopts to compute the forecasting losses in the subsequent week. Thus, since the system does not account for structural retrofitting, the percentage numbers of collapsed buildings cannot reduce in any of the subsequent days of Figure 7.

As shown, in the municipalities closest to the epicentres of the sequence, a larger percentage of buildings is estimated to be damaged after the earthquakes occurred on the 06th of April: 15% of the buildings are estimated to be in pl_2, 8% in pl_3, 5% in pl_4, 65% in pl_5, and only the 6% of the buildings result as undamaged. This implies, for example, that the value of 67% of collapsed buildings with 10km forecasted by MANTIS v2.0 on the 7th of April (see Figure 6) is obtained considering that 65% of the buildings are estimated to be already collapsed at 00:00 of the day and the remaining 2% of buildings are expected to collapse in the subsequent week. Indeed, it is worth noting that the buildings expected to collapse in the same week by MANTIS-K v.1.1 are 2%. Referring to the same area, the variations of the estimated collapsed buildings due to the occurred earthquakes from the 8th to the 10th of April is minor (only one M5.4 earthquake occurred in that time interval).

Increasing the considered area, the percentage of undamaged buildings increases up to 91%, that is associated to the case of municipalities within 100km from the epicentres; thus, MANTIS v2.0 performs forecasts on an almost undamaged building portfolio, and the differences between the outcomes of MANTI-K and MANTIS v2.0 are mainly due to the update of the building portfolio.

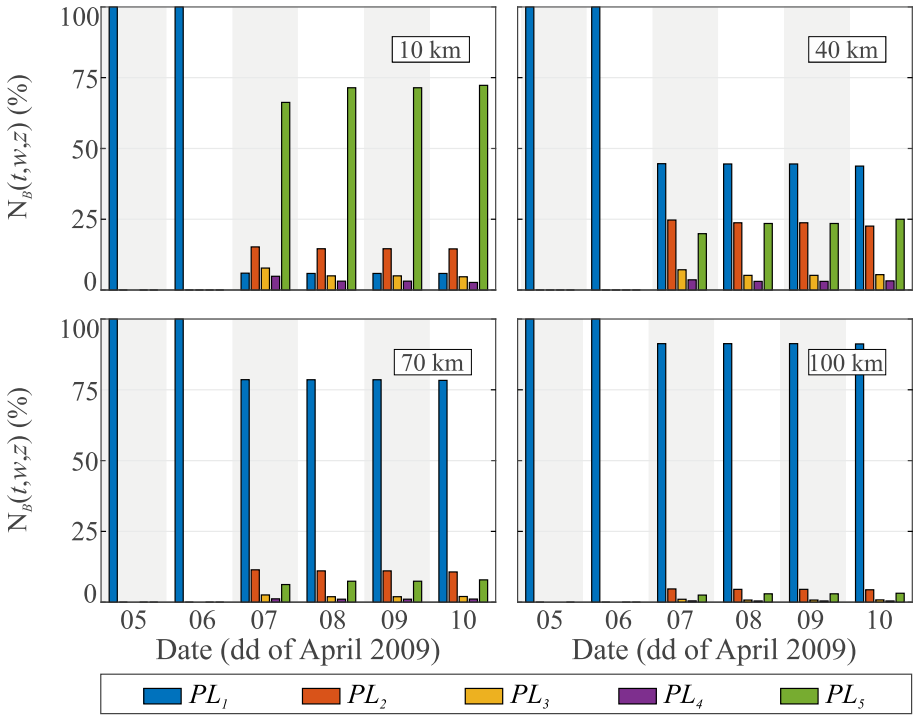

Figure 7 Building portfolio damage state at the days of prevision.

6. CONCLUSIONS AND DISCUSSION

MANTIS-K, an Italian system for operational earthquake loss forecasting, was formulated to convert the weekly seismic rates provided by an operational earthquake forecasting system into weekly seismic risk metrics. However, MANTIS-K, in its original formulation, is not able to account for structural damage accumulation and this limitation could lead to underestimate the forecasted losses during a seismic sequence. Thus, with the aim of upgrading the existing Italian OELF system, a new version, named MANTIS v2.0, is under-development.

Starting from the same seismic rates adopted by MANTIS-K, MANTIS v2.0 is intended to extend at the structural typologies, a methodology previously developed for single-structure reliability accounting for damage accumulation. Such a methodology is based on the hypothesis of Markovian evolution of structural seismic damage, i.e., the evolution of the damage due to an earthquake depends on the intensity of the earthquake and on the structural damage condition (i.e., performance level) when the earthquake occurs. Thus, accepting the same Markovian hypothesis, it was shown how, knowing the fragility function and state-dependent fragility functions for structural typologies, together with the number of buildings in each structural typologies, the formulated methodology provides measures of forecasted losses accounting for two sources of damage accumulation, both neglected in MANTIS-K: (i) damaged accumulation due to the (possible) occurrence of more than one earthquake in the forecasting time-window; (ii) the structural damages produced by the earthquakes occurred before the computation time.

With respect to MANTIS-K, the methodology requires to substitute the fragility functions used in MANTIS-K with the state-dependent fragility functions. The same seismic rates and inventory models are used by both MANTIS-K and MANTIS v2.0 as input information, but MANTIS v2.0 is able to update the inventory models accounting for the available information about the occurred earthquakes.

The 2009 L'Aquila 2009 seismic swarm was retrospectively analyzed by both the versions of the OELF system. The comparison of the results shows that by neglecting the possibility to have damage cumulation during a seismic swarm and the possibility to update the building portfolio according to the observed earthquake of the sequence leads to an underestimation of the forecasted losses, especially when the area of analysis is small and close to the epicenters of the sequence, i.e., it is supposed to be heavily damaged by the occurred shocks.

Appendix A

This appendix discusses the way in which the conditional distribution of $Sa_{avg}(\mathbf{T})$ can be computed in two alternative cases (symbology of this section is in accordance with the rest of the document). In the first case, the magnitude and the location of the earthquake are known and a GMPE providing the conditional distributions of the spectral accelerations associated to all the vibration periods collected in the vector $\mathbf{T}$ is at hand. This case is the of interest for Section 4.1.1. In the second case, apart from magnitude and location of the (occurred earthquake), and the GMPE, the values of the spectral accelerations at three periods (indicated by the vector $\mathbf{T}^* = \{0, 0.3, 1\}$ *s*) are known. This case is related to Section 4.1.5.

It is assumed that the logarithms of the spectral ordinates at the site of interest, given magnitude, m^*, and distance (i.e., location), r^*, of the earthquake, are jointly Gaussian, that is, they follow a multivariate normal distribution. It follows that, conditional to magnitude and distance, $\ln Sa_{\text{avg}}(\mathbf{T})$ is also normally distributed and Eqs. (16) and (17) provide the conditional logarithmic mean, $E\left[\ln Sa_{avg}(\mathbf{T}) \mid m^*, r^*, \theta_q\right]$, and the variance, $Var\left[\ln Sa_{avg}(\mathbf{T})\right]$, of $\ln Sa_{avg}(\mathbf{T})$ for a given value of m^*, r^* and soil condition, θ_q:

$$E\left[\ln Sa_{avg}(\mathbf{T}) \mid m^*, r^*, \theta_q\right] = \begin{bmatrix} \frac{1}{L} & \frac{1}{L} & \cdots & \frac{1}{L} \end{bmatrix} \begin{bmatrix} E\left[\ln Sa(T_1) \mid m^*, r^*, \theta_q\right] \\ E\left[\ln Sa(T_2) \mid m^*, r^*, \theta_q\right] \\ \vdots \\ E\left[\ln Sa(T_L) \mid m^*, r^*, \theta_q\right] \end{bmatrix}, \tag{16}$$

$$Var\left[\ln Sa_{avg}(\mathbf{T})\right] = \begin{bmatrix} \frac{1}{L} & \frac{1}{L} & \cdots & \frac{1}{L} \end{bmatrix} \begin{bmatrix} (\sigma_1)^2 & \rho_{1,2}\cdot\sigma_1\cdot\sigma_2 & \cdots & \rho_{1,L}\cdot\sigma_1\cdot\sigma_L \\ \rho_{2,1}\cdot\sigma_2\cdot\sigma_1 & (\sigma_2)^2 & \cdots & \rho_{2,L}\cdot\sigma_2\cdot\sigma_L \\ \vdots & \vdots & \ddots & \vdots \\ \rho_{L,1}\cdot\sigma_L\cdot\sigma_1 & \rho_{L,2}\cdot\sigma_L\cdot\sigma_2 & \cdots & (\sigma_L)^2 \end{bmatrix} \begin{bmatrix} \frac{1}{L} \\ \frac{1}{L} \\ \vdots \\ \frac{1}{L} \end{bmatrix}. \tag{17}$$

In Eq. (16), $E\left[\ln Sa(T_l) \mid m^*, r^*, \theta_q\right]$ is the expected value of the logarithm of spectral acceleration at the period T_l as specified by the GMPE with $l = 1, \ldots, L$; in Eq. (17), $\rho_{h,l}$ is the spectral correlation coefficient between two spectral ordinates with $l = 1, \ldots, L$ and $h = 1, \ldots, L$ and it is given by Baker & Jayaram (2008); σ_l is the standard deviation of $\ln Sa(T_l)$ as provided by the GMPE with $l = 1, \ldots, L$. Applying Eqs. (16) and (17), the $f_{IM|M,R,\theta_q}\left(im \mid m, r, \theta_q\right)$ distribution of Eq. (4) can be computed being $Sa_{avg}(\mathbf{T})$ the chosen IM.

Let us know consider that, according to data retrieved from the ShakeMap, the values of the spectra acceleration for three vibration periods, $\mathbf{T}^* = \{0, 0.3, 1\}$ *s*, are assumed as known. It is possible to evaluate the logarithm of the geometric mean of the pseudo-spectral accelerations, $\ln Sa_{avg}(\mathbf{T}^*) = \chi$. The distribution of $Sa_{avg}(\mathbf{T})$ conditioned to the occurrence of a given value of m^*, r^*, θ_q and χ is defined by its conditional mean, $E\left[\ln Sa_{avg}(\mathbf{T}) \mid m^*, r^*, \theta_q, \chi\right]$, and variance, $VAR\left[\ln Sa_{avg}(\mathbf{T}) \mid \chi\right]$, evaluated via Eqs. (18) and (19), respectively:

$$\begin{aligned} E\left[\ln Sa_{avg}(\mathbf{T}) \mid m^*, r^*, \theta_q, \chi\right] &= E\left[\ln Sa_{avg}(\mathbf{T}) \mid m^*, r^*, \theta_q\right] + \\ &+ \rho\left[\ln Sa_{avg}(\mathbf{T}), \ln Sa_{avg}(\mathbf{T}^*)\right] \cdot \frac{\sigma_{\ln Sa_{avg}(\mathbf{T})}}{\sigma_{\ln Sa_{avg}(\mathbf{T}^*)}} \cdot \left(\chi - E\left[\ln Sa_{avg}(\mathbf{T}^*) \mid m^*, r^*, \theta_q\right]\right), \end{aligned} \tag{18}$$

$$VAR\left[\ln Sa_{avg}(\mathbf{T}) \mid \chi\right] = VAR\left[\ln Sa_{avg}(\mathbf{T}^*)\right] \cdot \left[1 - \left(\rho\left[\ln Sa_{avg}(\mathbf{T}), \ln Sa_{avg}(\mathbf{T}^*)\right]\right)^2\right], \tag{19}$$

where $E\left[\ln Sa_{avg}\left(\mathbf{T}^*\right)|\, m^*, r^*, \theta_q\right]$ and $VAR\left[\ln Sa_{avg}\left(\mathbf{T}^*\right)\right]$ can be evaluated as per Eqs. (16) and (17) by substituting the set of the periods in $\mathbf{T}$ with those in $\mathbf{T}^*$, and $\rho\left[\ln Sa_{avg}(\mathbf{T}), \ln Sa_{avg}\left(\mathbf{T}^*\right)\right]$ is the correlation coefficient provided by Eq. (20):

$$\rho\left[\ln Sa_{avg}(\mathbf{T}), \ln Sa_{avg}\left(\mathbf{T}^*\right)\right] = \frac{COV\left[\ln Sa_{avg}(\mathbf{T}), \ln Sa_{avg}\left(\mathbf{T}^*\right)\right]}{\sqrt{VAR\left[\ln Sa_{avg}(\mathbf{T})\right] \cdot VAR\left[\ln Sa_{avg}\left(\mathbf{T}^*\right)\right]}}. \tag{20}$$

The numerator of Eq. (20) can be computed by Eq. (21) (see Iervolino, 2021 for details):

$$COV\left[\ln Sa_{avg}(\mathbf{T}), \ln Sa_{avg}\left(\mathbf{T}^*\right)\right] =$$

$$= \begin{bmatrix} \frac{1}{L} & \frac{1}{L} & \cdots & \frac{1}{L} \end{bmatrix} \begin{bmatrix} (\sigma_1)^2 & \rho_{1,2}\cdot\sigma_1\cdot\sigma_2 & \rho_{1,3}\cdot\sigma_1\cdot\sigma_3 \\ \rho_{2,1}\cdot\sigma_2\cdot\sigma_1 & (\sigma_2)^2 & \rho_{2,3}\cdot\sigma_2\cdot\sigma_3 \\ \vdots & \vdots & \vdots \\ \rho_{L,1}\cdot\sigma_L\cdot\sigma_1 & \rho_{L,2}\cdot\sigma_L\cdot\sigma_2 & \rho_{L,3}\cdot\sigma_L\cdot\sigma_3 \end{bmatrix} \begin{bmatrix} \frac{1}{3} \\ \frac{1}{3} \\ \frac{1}{3} \end{bmatrix}. \tag{21}$$

Eqs. (18) from (21) allow computing the conditional distribution adopted in Eq. (9).

Appendix B

The adopted set of building-classes includes five different construction materials, that is reinforced concrete (CR) in which the load resisting frame are infilled frame (LFINF), and rubble stone masonry (MUR-STRUB), clay brick masonry (MUR-CL99), dressed stone masonry (MUR-STDRE) or confined masonry (MCF) for which the load resisting frame are load bearing walls (LWAL). Masonry structures are non-ductile structures or low ductility structures (DNO and DUL respectively), while reinforced concrete structures were designed in absence of seismic design (CDN) or according to low code design level (CDL), that is, they are designed for lateral resistance using allowable stress design. For RC, the value of the lateral force coefficient, i.e., the fraction of the weight that was specified as the design lateral force in the seismic design code, can be 0, 5 or 10. Finally, the building-classes vary the number of the story (H) from 1 to 6.
For these building-classes RISE project provides the fundamental period and the linearized capacity curves in terms of displacement (d) and base shear over the mass (F/m), as shown in the Figure 8. Example of capacity curve and definition of *PLs*. The subscripts *y*, *c*, *p* and *u* denote, in turn, the yielding-point, the capping-point, the residual-point and the ultimate-capacity-point.

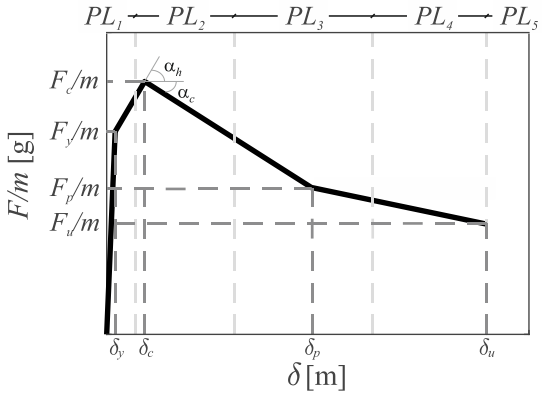

Figure 8. Example of capacity curve and definition of *PLs*. The subscripts *y*, *c*, *p* and *u* denote, in turn, the yielding-point, the capping-point, the residual-point and the ultimate-capacity-point.

In Table 2 the capacity curves parameters of the considered building-classes are reported. F_y and d_y are the yield base share and the yield displacement, respectively; μ_c is the capping-point ductility (i.e., the ratio between the capping-point displacement and the yielding point displacement); a_h and a_c are the hardening and the post-capping slopes, respectively; r_p is the ratio of residual base share divided by yield base share; μ_f is the ultimate displacement capacity over the yield displacement; finally, T_y is the fundamental period.
The fragility functions and the state-dependent fragility functions (defined by the mean, η, and the standard deviation, β, of the lognormal) for each building-classes are reported in Table 3 and Table 4, respectively. In the tables, the taxonomy of the building-class ID is such that: i) construction material; ii) lateral load resisting frame; iii) ductility design level for the masonry structures or code design level for the reinforced concrete structures; iv) number of the stories; v) value of the lateral force coefficient expressed in percentage.

Table 2. Parameters of building-classes capacity curves.

ID building-class	F_y	δ_y	α_h	μ_c	α_c	r_p	μ_f	T_y
MUR-STRUB_ LWAL-DNO_H1	1.913	0.00030	0.18	6.71	0.00076	2.02	33.56	0.16
MUR-STRUB_ LWAL-DNO_H2	1.099	0.00060	0.14	8.40	0.00106	2.03	33.61	0.29
MUR-STRUB_ LWAL-DNO_H3	0.795	0.00089	0.15	7.85	0.00092	2.02	34.75	0.42
MUR-STRUB_ LWAL-DNO_H4	0.628	0.00119	0.14	8.40	0.00060	2.03	34.45	0.55
MUR-STRUB_ LWAL-DNO_H5	0.530	0.00149	0.14	8.06	0.00071	2.02	34.27	0.67
MUR-CL99_ LWAL-DNO_H3	0.804	0.00100	0.14	8.02	0.00094	2.02	34.10	0.44

MUR-CL99_ LWAL-DNO_H4	0.638	0.00133	0.14	8.27	0.00058	2.03	34.59	0.57
MUR-CL99_ LWAL-DNO_H5	0.540	0.00166	0.14	7.82	0.00069	2.00	34.30	0.70
MUR-STDRE_ LWAL-DNO_H4	0.667	0.00126	0.14	7.94	0.00112	2.03	34.13	0.55
MUR-STDRE_ LWAL-DNO_H5	0.559	0.00158	0.14	8.25	0.00067	2.02	34.29	0.67
MCF_LWAL-DUL_H1	4.611	0.00044	0.12	9.03	0.00073	2.02	38.37	0.12
MCF_LWAL-DUL_H2	2.305	0.00089	0.15	7.89	0.00070	2.02	38.33	0.25
MCF_LWAL-DUL_H3	1.540	0.00133	0.14	8.27	0.00087	2.02	37.59	0.37
MCF_LWAL-DUL_H4	1.158	0.00177	0.14	7.90	0.00057	2.01	37.79	0.49
MCF_LWAL-DUL_H5	0.922	0.00222	0.14	8.12	0.00071	2.02	37.89	0.62
CR_LFINF-CDN_H1_0	2.866	0.00166	0.06	5.30	-0.01781	0.67	57.52	0.15
CR_LFINF-CDN_H2_0	1.345	0.00293	0.07	4.60	-0.03034	0.82	29.29	0.29
CR_LFINF-CDN_H3_0	1.005	0.00497	0.07	4.77	-0.04592	0.85	19.73	0.44
CR_LFINF-CDN_H4_0	0.801	0.00726	0.06	4.99	-0.05877	0.88	14.82	0.60
CR_LFINF-CDN_H5_0	0.741	0.01007	0.07	4.68	-0.07305	0.91	12.23	0.73
CR_LFINF-CDN_H6_0	0.701	0.01364	0.07	4.54	-0.08767	0.93	10.31	0.88
CR_LFINF-CDL_H1_5	3.281	0.00193	0.07	4.60	-0.02577	0.70	45.96	0.15
CR_LFINF-CDL_H2_5	1.372	0.00327	0.08	4.07	-0.03492	0.79	25.42	0.31
CR_LFINF-CDL_H3_5	1.035	0.00539	0.08	3.96	-0.05687	0.79	16.43	0.45
CR_LFINF-CDL_H4_5	0.896	0.00822	0.10	3.62	-0.08606	0.84	10.88	0.60
CR_LFINF-CDL_H5_5	0.841	0.01116	0.12	3.04	-0.12993	0.84	8.11	0.72
CR_LFINF-CDL_H6_5	0.840	0.01476	0.14	2.75	-0.17942	0.87	6.19	0.83
CR_LFINF-CDL_H1_10	3.249	0.00193	0.07	4.61	-0.02495	0.70	46.47	0.15
CR_LFINF-CDL_H2_10	1.399	0.00338	0.08	4.12	-0.03683	0.79	25.72	0.31
CR_LFINF-CDL_H3_10	1.255	0.00627	0.09	3.66	-0.06469	0.80	16.40	0.44
CR_LFINF-CDL_H4_10	1.103	0.00944	0.12	3.01	-0.10194	0.82	10.58	0.58
CR_LFINF-CDL_H5_10	1.008	0.01254	0.16	2.53	-0.13685	0.80	8.87	0.70
CR_LFINF-CDL_H6_10	1.001	0.01619	0.16	2.52	-0.18343	0.85	6.19	0.80

Table 3. Parameters of fragility functions.

ID building class	Lognornal parameters	PL_2	PL_3	PL_4	PL_5
MUR-STRUB_LWAL-DNO_H1	η	-2.47	-2.04	-1.82	-1.70
	β	0.26	0.22	0.18	0.17
MUR-STRUB_LWAL-DNO_H2	η	-2.88	-2.33	-2.04	-1.85
	β	0.21	0.25	0.28	0.30

MUR-STRUB_LWAL-DNO_H3	η	-2.92	-2.27	-1.92	-1.70
	β	0.30	0.33	0.38	0.42
MUR-STRUB_LWAL-DNO_H4	η	-2.91	-2.22	-1.87	-1.66
	β	0.37	0.42	0.45	0.47
MUR-STRUB_LWAL-DNO_H5	η	-2.87	-2.17	-1.79	-1.57
	β	0.40	0.46	0.48	0.47
MUR-CL99_LWAL-DNO_H3	η	-2.86	-2.23	-1.88	-1.66
	β	0.33	0.34	0.40	0.43
MUR-CL99_LWAL-DNO_H4	η	-2.85	-2.14	-1.79	-1.58
	β	0.37	0.43	0.46	0.47
MUR-CL99_LWAL-DNO_H5	η	-2.80	-2.08	-1.71	-1.49
	β	0.41	0.46	0.47	0.48
MUR-STDRE_LWAL-DNO_H4	η	-2.87	-2.14	-1.80	-1.58
	β	0.36	0.40	0.44	0.47
MUR-STDRE_LWAL-DNO_H5	η	-2.79	-2.11	-1.74	-1.52
	β	0.41	0.46	0.47	0.47
MCF_LWAL-DUL_H1	η	-1.91	-1.52	-1.31	-1.19
	β	0.25	0.20	0.18	0.18
MCF_LWAL-DUL_H2	η	-2.23	-1.63	-1.34	-1.18
	β	0.21	0.22	0.24	0.26
MCF_LWAL-DUL_H3	η	-2.38	-1.73	-1.40	-1.18
	β	0.27	0.31	0.35	0.41
MCF_LWAL-DUL_H4	η	-2.41	-1.68	-1.31	-1.09
	β	0.34	0.38	0.43	0.46
MCF_LWAL-DUL_H5	η	-2.39	-1.64	-1.26	-1.04
	β	0.37	0.46	0.46	0.47
CR_LFINF-CDN_H1_0	η	-1.06	-0.48	-0.27	-0.12
	β	0.27	0.16	0.18	0.24
CR_LFINF-CDN_H2_0	η	-1.69	-1.04	-0.78	-0.68
	β	0.21	0.24	0.28	0.31
CR_LFINF-CDN_H3_0	η	-1.68	-1.10	-0.86	-0.78
	β	0.29	0.31	0.37	0.39
CR_LFINF-CDN_H4_0	η	-1.57	-1.12	-0.87	-0.79
	β	0.35	0.38	0.44	0.45
CR_LFINF-CDN_H5_0	η	-1.53	-1.05	-0.84	-0.76
	β	0.37	0.46	0.46	0.46
CR_LFINF-CDN_H6_0	η	-1.40	-0.99	-0.78	-0.73
	β	0.43	0.47	0.48	0.46
CR_LFINF-CDL_H1_5	η	-0.96	-0.45	-0.27	-0.11
	β	0.29	0.16	0.14	0.22
CR_LFINF-CDL_H2_5	η	-1.72	-1.05	-0.79	-0.68
	β	0.21	0.24	0.28	0.31

CR_LFINF-CDL_H3_5	η	-1.77	-1.17	-0.92	-0.84
	β	0.28	0.31	0.35	0.37
CR_LFINF-CDL_H4_5	η	-1.71	-1.24	-1.01	-0.94
	β	0.34	0.36	0.39	0.43
CR_LFINF-CDL_H5_5	η	-1.75	-1.29	-1.07	-0.98
	β	0.35	0.38	0.42	0.47
CR_LFINF-CDL_H6_5	η	-1.71	-1.28	-1.05	-1.00
	β	0.40	0.43	0.45	0.47
CR_LFINF-CDL_H1_10	η	-0.99	-0.46	-0.27	-0.10
	β	0.29	0.16	0.14	0.22
CR_LFINF-CDL_H2_10	η	-1.67	-1.03	-0.76	-0.64
	β	0.22	0.25	0.28	0.31
CR_LFINF-CDL_H3_10	η	-1.64	-1.02	-0.78	-0.65
	β	0.28	0.30	0.34	0.37
CR_LFINF-CDL_H4_10	η	-1.70	-1.12	-0.89	-0.78
	β	0.35	0.35	0.36	0.41
CR_LFINF-CDL_H5_10	η	-1.76	-1.16	-0.91	-0.78
	β	0.35	0.37	0.42	0.45
CR_LFINF-CDL_H6_10	η	-1.67	-1.19	-0.97	-0.87
	β	0.38	0.42	0.45	0.45

Table 4. Parameters of state-dependent fragility functions.

	Lognormal parameters	PL_2 PL_3	PL_2 PL_4	PL_2 PL_5	PL_3 PL_4	PL_3 PL_5	PL_4 PL_5
MUR-STRUB_LWAL-DNO_H1	η	-2.312	-1.948	-1.775	-3.168	-2.484	-3.519
	β	0.257	0.199	0.183	0.436	0.392	0.443
MUR-STRUB_LWAL-DNO_H2	η	-2.948	-2.250	-1.986	-3.321	-2.663	-3.471
	β	0.381	0.305	0.302	0.440	0.424	0.545
MUR-STRUB_LWAL-DNO_H3	η	-2.693	-2.107	-1.819	-3.125	-2.456	-3.266
	β	0.414	0.371	0.406	0.482	0.470	0.586
MUR-STRUB_LWAL-DNO_H4	η	-2.760	-2.088	-1.785	-3.038	-2.420	-3.052
	β	0.455	0.442	0.456	0.575	0.529	0.665
MUR-STRUB_LWAL-DNO_H5	η	-2.623	-1.991	-1.680	-2.915	-2.245	-2.929
	β	0.489	0.475	0.476	0.581	0.542	0.765
MUR-CL99_LWAL-DNO_H3	η	-2.709	-2.078	-1.789	-3.082	-2.415	-3.159
	β	0.440	0.388	0.418	0.485	0.484	0.575
MUR-CL99_LWAL-DNO_H4	η	-2.704	-2.012	-1.711	-2.943	-2.305	-2.986
	β	0.483	0.462	0.464	0.596	0.543	0.712
MUR-CL99_LWAL-DNO_H5	η	-2.525	-1.906	-1.588	-2.834	-2.171	-2.832
	β	0.485	0.480	0.479	0.618	0.567	0.721
MUR-STDRE_LWAL-DNO_H4	η	-2.587	-1.981	-1.690	-2.965	-2.324	-2.979
	β	0.443	0.434	0.448	0.556	0.517	0.650
MUR-STDRE_LWAL-DNO_H5	η	-2.607	-1.957	-1.637	-2.849	-2.214	-2.862
	β	0.494	0.478	0.476	0.630	0.566	0.762

MCF_LWAL-DUL_H1	η	-2.126	-1.516	-1.300	-2.736	-2.121	-2.997
	β	0.328	0.208	0.189	0.364	0.340	0.418
MCF_LWAL-DUL_H2	η	-2.025	-1.498	-1.267	-2.687	-2.022	-2.879
	β	0.273	0.255	0.265	0.422	0.434	0.559
MCF_LWAL-DUL_H3	η	-2.193	-1.586	-1.304	-2.635	-1.961	-2.767
	β	0.389	0.348	0.382	0.504	0.472	0.587
MCF_LWAL-DUL_H4	η	-2.054	-1.481	-1.191	-2.501	-1.840	-2.518
	β	0.420	0.419	0.441	0.562	0.523	0.644
MCF_LWAL-DUL_H5	η	-2.083	-1.459	-1.154	-2.407	-1.733	-2.380
	β	0.476	0.465	0.472	0.601	0.572	0.743
CR_LFINF-CDN_H1_0	η	-0.59	-0.33	-0.17	-1.28	-0.56	-1.53
	β	0.18	0.20	0.25	0.45	0.35	0.63
CR_LFINF-CDN_H2_0	η	-1.21	-0.86	-0.72	-1.81	-1.12	-1.92
	β	0.28	0.29	0.32	0.49	0.41	0.53
CR_LFINF-CDN_H3_0	η	-1.47	-1.01	-0.82	-1.90	-1.26	-2.28
	β	0.38	0.36	0.40	0.54	0.48	1.55
CR_LFINF-CDN_H4_0	η	-1.76	-1.13	-0.90	-1.99	-1.45	-2.24
	β	0.51	0.43	0.44	0.62	0.54	0.74
CR_LFINF-CDN_H5_0	η	-1.73	-1.10	-0.87	-1.96	-1.41	-2.07
	β	0.58	0.47	0.45	0.63	0.57	0.69
CR_LFINF-CDN_H6_0	η	-1.72	-1.11	-0.86	-1.91	-1.41	-2.12
	β	0.59	0.49	0.46	0.66	0.60	0.76
CR_LFINF-CDL_H1_5	η	-0.57	-0.34	-0.16	-1.34	-0.62	-1.57
	β	0.18	0.15	0.22	0.46	0.37	0.54
CR_LFINF-CDL_H2_5	η	-1.22	-0.87	-0.73	-1.87	-1.16	-2.12
	β	0.27	0.29	0.32	0.56	0.42	0.64
CR_LFINF-CDL_H3_5	η	-1.47	-1.05	-0.89	-1.95	-1.31	-2.13
	β	0.37	0.35	0.39	0.54	0.46	0.64
CR_LFINF-CDL_H4_5	η	-1.67	-1.18	-0.98	-2.06	-1.48	-2.29
	β	0.44	0.40	0.43	0.64	0.54	0.67
CR_LFINF-CDL_H5_5	η	-1.64	-1.20	-1.03	-2.04	-1.51	-2.49
	β	0.47	0.43	0.46	0.59	0.53	1.09
CR_LFINF-CDL_H6_5	η	-1.66	-1.23	-1.06	-2.01	-1.52	-2.36
	β	0.53	0.47	0.46	0.60	0.55	0.65
CR_LFINF-CDL_H1_10	η	-0.58	-0.34	-0.15	-1.32	-0.60	-1.52
	β	0.18	0.16	0.23	0.43	0.37	0.49
CR_LFINF-CDL_H2_10	η	-1.20	-0.84	-0.70	-1.80	-1.11	-2.00
	β	0.27	0.29	0.32	0.60	0.44	0.56
CR_LFINF-CDL_H3_10	η	-1.27	-0.88	-0.70	-1.79	-1.12	-1.97
	β	0.35	0.35	0.39	0.50	0.45	0.62
CR_LFINF-CDL_H4_10	η	-1.41	-1.01	-0.83	-1.85	-1.24	-1.99
	β	0.39	0.39	0.43	0.53	0.48	0.68

CR_LFINF-CDL_H5_10	η	-1.32	-0.96	-0.81	-1.86	-1.23	-2.19
	β	0.41	0.44	0.45	0.57	0.51	0.98
CR_LFINF-CDL_H6_10	η	-1.46	-1.07	-0.93	-1.89	-1.38	-2.21
	β	0.46	0.45	0.47	0.62	0.54	0.72

7. References

Baker, J. W., & Cornell, C. A. (2006). Spectral shape, epsilon and record selection. *Earthquake Engineering & Structural Dynamics*, *35*(9), 1077–1095. https://doi.org/10.1002/eqe.571

Baker, J. W., & Jayaram, N. (2008). Correlation of spectral acceleration values from NGA ground motion models. *Earthquake Spectra*, *24*(1), 299–317. https://doi.org/10.1193/1.2857544

Bindi, D., Pacor, F., Luzi, L., Puglia, R., Massa, M., Ameri, G., & Paolucci, R. (2011). Ground motion prediction equations derived from the Italian strong motion database. *Bulletin of Earthquake Engineering*, *9*(6), 1899–1920. https://doi.org/10.1007/s10518-011-9313-z

Chioccarelli, E., & Iervolino, I. (2010). Near-source seismic demand and pulse-like records: A discussion for L'Aquila earthquake. *Earthquake Engineering and Structural Dynamics*, *39*(2), 1039–1062. https://doi.org/10.1002/eqe

Chioccarelli, E., & Iervolino, I. (2021). Comparing short-term seismic and COVID-19 fatality risks in Italy. *Seismological Research Letters*, *92*(4), 2382–2388. https://doi.org/10.1785/0220200368

Forte, G., Chioccarelli, E., de Falco, M., Cito, P., Santo, A., & Iervolino, I. (2019). Seismic soil classification of Italy based on surface geology and shear-wave velocity measurements. *Soil Dynamics and Earthquake Engineering*, *122*(3), 79–93. https://doi.org/10.1016/j.soildyn.2019.04.002

Gutenberg, B., & Richter, C. F. (1944). Frequency of earthquakes in California. *Bulletin of the Seismological Society of America*, *34*(4), 185–188. https://doi.org/10.1785/bssa0340040185

Iervolino, I. (2021). *Dinamica delle strutture e ingegneria sismica. Principi e applicazioni*. Hoepli.

Iervolino, I., Chioccarelli, E., Giorgio, M., Marzocchi, W., Zuccaro, G., Dolce, M., & Manfredi, G. (2015). Operational (short-term) earthquake loss forecasting in Italy. *Bulletin of the Seismological Society of America*, *105*(4), 2286–2298. https://doi.org/10.1785/0120140344

Iervolino, I., Giorgio, M., & Chioccarelli, E. (2016). Markovian modeling of seismic damage accumulation. *Earthquake Engineering and Structural Dynamics*, *45*(3), 441–461. https://doi.org/10.1002/eqe.2668

Jordan, T. H., Chen, Y. T., Gasparini, P., Madariaga, R., Main, I., Marzocchi, W., Papadopoulos, G., Sobolev, G., Yamaoka, K., & Zschau, J. (2011). Operational earthquake forecasting: State of knowledge and guidelines for utilization. *Annals of Geophysics*, *54*(4), 319–391. https://doi.org/10.4401/ag-5350

Lagomarsino, S., & Giovinazzi, S. (2006). Macroseismic and mechanical models for the vulnerability and damage assessment of current buildings. *Bulletin of Earthquake Engineering*, *4*(4), 415–443. https://doi.org/10.1007/s10518-006-9024-z

Marzocchi, W., Iervolino, I., Giorgio, M., & Falcone, G. (2015). When is the probability of a large Earthquake too small? *Seismological Research Letters*, *86*(6), 1674–1678. https://doi.org/10.1785/0220150129

Marzocchi, W., & Lombardi, A. M. (2009). Real-time forecasting following a damaging earthquake. *Geophysical Research Letters*, *36*(21), 1–5. https://doi.org/10.1029/2009GL040233

Marzocchi, W., Lombardi, A. M., & Casarotti, E. (2014). The establishment of an operational earthquake forecasting system in Italy. *Seismological Research Letters*, *85*(5), 961–969. https://doi.org/10.1785/0220130219

Orlacchio, M., Chioccarelli, E., Baltzopoulos, G., & Iervolino, I. (2021). State-Dependent Seismic Fragility Functions for Italian Reinforced Concrete Structures: Preliminary Results. *31th European Safety and Reliability Conference, 19-23 September 2021, Angers, France*, 1591–1598. https://doi.org/10.3850/978-981-18-2016-8_660-cd

Pacifico, A., Chioccarelli, E., & Iervolino, I. (2022). Residential code-conforming structural seismic risk maps for Italy. *Soil Dynamics and Earthquake Engineering*, *153*, 1–13. https://doi.org/10.1016/j.soildyn.2021.107104

Romão, X., Castro, J. M., Peirera, N., Crowley, H., Silva, V., Martins, L., & Rodrigues, D. (2019). *Project SERA. Deliverable 26.5: European physical vulnerability models*.

Suzuki, A., & Iervolino, I. (2019). Seismic Fragility of Code-conforming Italian Buildings Based on SDoF Approximation. *Journal of Earthquake Engineering*. https://doi.org/10.1080/13632469.2019.1657989

Villar-Vega, M., Silva, V., Eeri, M., Crowley, H., & Catalina, Y. (2017). Assessment of earthquake damage considering the characteristics of past events in South America. *Soil Dynamics and Earthquake Engineering*, *99*(March), 86–96. https://doi.org/10.1016/j.soildyn.2017.05.004

Wald, D. J., Quitoriano, V., Heaton, T. H., Kanamori, H., Scrivner, C. W., & Worden, C. B. (1999). TriNet "ShakeMaps": Rapid generation of peak ground motion and intensity maps for earthquakes in southern California. *Earthquake Spectra*, *15*(3), 537–554. https://doi.org/10.1193/1.1586057

Wang, K., & Rogers, G. C. (2014). Earthquake preparedness should not fluctuate on a daily or weekly basis. *Seismological Research Letters*, *85*(3), 569–571. https://doi.org/https://doi.org/10.1785/0220130195

Worden, C. B., Thompson, E. M., Hearne, M., & Wald, D. J. (2020). *ShakeMap Manual Online: Technical Manual, User's Guide, and Software Guide*. https://doi.org/10.5066/F7D21VPQ

This project has received funding from the European Union's Horizon 2020 research and innovation programme under grant agreement No 821115.